J. Hydrol. Hydromech., 67, 2019, 4, 384–392
DOI: 10.2478/johh-2019-0017

# Predicting impacts of climate change on evapotranspiration and soil moisture for a site with subhumid climate

András Herceg[1*], Reinhard Nolz[2], Péter Kalicz[1], Zoltán Gribovszki[1]

[1] University of Sopron, Institute of Geomatics and Civil Engineering, Bajcsy-Zsilinszky s. 4, Sopron H-9400, Hungary.
[2] University of Natural Resources and Life Sciences, Vienna, Institute of Hydraulics and Rural Water Management, Muthgasse 18, 1190 Wien, Austria.
[*] Corresponding author. Tel.: +36 30 719 4527. E-mail: herceg.andras88@gmail.com

**Abstract:** The current and ongoing climate change over Europe can be characterized by statistically significant warming trend in all seasons. Warming has also an effect on the hydrological cycle through the precipitation intensity. Consequently, the supposed changes in the distribution and amount of precipitation with the continuously increasing temperature may induce a higher rate in water consumption of the plants, thus the adaptation of the plants to the climate change can be critical. The hydrological impact of climate change was studied based on typical environmental conditions of a specific agricultural area in Austria. For this purpose, (1) a monthly step, Thornthwaite-type water balance model was established and (2) the components of the water balance were projected for the 21st century, both (a) with a basic rooting depth condition (present state) and (b) with a (hypothetically) extended rooting depth (in order to evaluate potential adaption strategies of the plants to the warming). To achieve the main objectives, focus was set on calibrating and validating the model using local reference data. A key parameter of the applied model was the water storage capacity of the soil ($SOIL_{MAX}$), represented in terms of a maximum rooting depth. The latter was assessed and modified considering available data of evapotranspiration and soil physical properties. The adapted model was utilized for projections on the basis of four bias corrected Regional Climate Models. An extended rooting depth as a potential adaptation strategy for effects of climate change was also simulated by increasing $SOIL_{MAX}$. The basic simulation results indicated increasing evapotranspiration and soil moisture annual mean values, but decreasing minimum soil moisture for the 21st century. Seasonal examination, however, revealed that a decrease in soil moisture may occur in the growing season towards to the end of the 21st century. The simulations suggest that the vegetation of the chosen agricultural field may successfully adapt to the water scarcity by growing their roots to the possibly maximum.

**Keywords:** Water balance; Plant available water; Weighing lysimeter; Regional Climate Model.

## INTRODUCTION

Climate change is mainly characterized by a global rise of average temperatures (global warming) and its subsequent impacts on the hydrological cycle. The average temperature already increased by 0.6°C during the 20th century, and is predicted to further increase during upcoming decades (IPCC, 2014). Baseline scenarios of global warming – such that do not consider mitigation effects – predict an increase of 3.7°C to 4.8°C by 2100 compared to pre-industrial levels. As increased temperatures also reflect a higher energy potential in the atmosphere, the resulting intensification of driving forces will influence the hydrological cycle. Expected effects include alteration of precipitation patterns and evapotranspiration processes at multiple scales (Sun et al., 2010). Consequently, extreme events in terms of thunderstorms as well as droughts are supposed to occur more often (IPCC, 2014). It is widely accepted that such massive impacts will considerably affect ecosystems and the services they provide for human well-being as, for example, food production. Against this background, it is necessary to evaluate impacts of climate change on the components of the water cycle (IPCC, 2007). According to the impact analysis studies of water balance models (e.g., Keables and Mehta, 2010; Lutz et al., 2010; Mohammed et al., 2012; Remrová and Císleřová, 2010), Zamfir (2014) demonstrated that the evapotranspiration may increase, but the soil water content may decrease in the future due to the presumably increasing temperature and the decreasing precipitation. Consequently, the occurrence of water scarcity may become more common towards the end of the 21st century.

The "Marchfeld" in the eastern part of Austria is one of the major field crop production area (covering about 1000 $km^2$ dominated by agricultural production), and nevertheless one of the driest region in Austria (Eitzinger et al., 2013). The region is characterized by a subhumid climate with a mean annual temperature and precipitation of approximately 10°C and 550 mm, respectively (Götz et al., 2000). Typical summers are hot and dry; winters are mainly cold with severe frost and limited snow cover (Götz et al., 2000). A typical soil type is Chernozem, a black-colored fertile soil (Götz et al., 2000). Despite the generally favorable environmental conditions, the region is prone to water deficit stress. Calculated reference evapotranspiration was on average 830 mm per year in the period 1990–2013 (after personal communication with Reinhard Nolz). Hence, irrigating agricultural fields has a long tradition to balance water deficit and ensure proper soil water conditions for crop production. For the future, irrigation is expected to become even more important for agricultural production in the "Marchfeld" because of climate change effects (Nachtnebel et al., 2014).

The researches on Marchfeld in context of water stress focus mainly on crop simulations (basically on winter wheat), e.g., Eitzinger et al. (2003, 2013), Strauss et al. (2012) and Thaler et al. (2012). However, some part of Marchfeld is grassland, and as we know none of the study has analyzed the effect of climate change on that grass covered surfaces until now. Therefore, the open question of this study was: How the water balance of grass covered areas may change in the future?

The main objective of this study was to upgrade and adjust the well-known water balance model after Thornthwaite to compute evapotranspiration and soil moisture based on simple and easily obtainable weather data (Dingman, 2002; Thornthwaite and Mather, 1955), and using high precision weighing lysimeter data (Nolz et al., 2016) for calibration and validation for local environmental conditions. Such an adjusted Thornthwaite-type water balance model was previously tested for a forest stand and for a mixed surface cover using MODIS data as calibration, for which it delivered proper results (Herceg et al., 2016). This study was also initiated to estimate future evapotranspiration and soil moisture under environmental conditions considered representative for the "Marchfeld".

The projection phase required weather data that were extracted from Regional Climate Models (RCMs) that were downscaled from Global Climate Models (GCMs). The dataset covered three periods in the 21st century (2015–2045; 2045–2075; 2070–2100). Considering predicted rainfall and evapotranspiration, soil moisture could be calculated based on a simple water balance. In doing so, two specific aspects were considered: In order to address the uncertainty of predictions (i.e., variations between different climate databases), the required model input was chosen from four different RCMs. The other aspect referred to plant water uptake and water deficit stress. For the simulations, two basic conditions were distinguished with respect to the rooting zone depth. The first run was based on a rooting depth corresponding to the rooting depht of the plants in the lysimeter during the calibration period (basic rooting depth of the plants). The second assumption was that plants were able to adapt to water stress conditions by increasing their rooting depth in order to suffice their needs taking advantage of a larger soil water reservoir (extended rooting depth of the plants).

In such a way, potential stress conditions were determined for both basic and extended rooting depth. Differences arising from varying soil characteristics as well as the changes of aboveground biomass were not considered in this study.

The new aspect of the study was on one hand the two-stage evapotranspiration calibration process (calibration of potential, and the calibration of the actual evapotranspiration separately), on second hand, the adaption of the broken-line regression method in the calibration of the potential evapotranspiration.

The main advantage of this model is the low amount of input data requirement (precipitation and temperature); therefore it could easily be extended to larger regional scale. The simplicity of this water-balance model ensures fast impact analysis of climate change on evapotranspiration and soil water storage, and requires a significant lower amount of work for input data' preprocessing for baseline investigations than more complex models. Nevertheless, the use of only two input parameters enables a much easier uncertainty analysis of the applied model.

## MATERIALS AND METHODS

### Study site and data base

Basic data for this study were obtained at the experimental farm of the University of Natural Resources and Life Sciences, Vienna (BOKU), in Groß-Enzersdorf (48°12'N, 16°34'E; 157 m). The location is regarded representative for the Marchfeld with respect to the climatic conditions. The experimental farm hosts a reference weather station of the Austrian "Zentralanstalt für Meteorologie und Geodynamik (ZAMG)" at which meteorological quantities were monitored according to the standard of the World Meteorological Organization (WMO). Data included air temperature, precipitation, relative humidity, global radiation, and wind velocity measured in 10 m height (Nolz et al., 2016).

Soil water balance components were determined using a single weighing lysimeter. It was installed at the experimental farm together with a second lysimeter in 1983 to study evapotranspiration at the surface, water content in the soil profile, and water drainage at the bottom outlet of the lysimeters (Neuwirth and Mottl, 1983). Its cylindrical vessel has an inner diameter of 1.9 m, a resulting surface area of 2.85 $m^2$, and a hemispherical bottom with a maximum depth of 2.5 m. During installation, a typical soil profile was created by re-packing soil in layers as follows:

- sandy loam soil (0–140 cm) (30% sand, 50% silt, 20% clay; porosity: 43%),
- gravel (140–250 cm) (mainly large pore sizes with negligible water holding capacity).

The soil characteristics and the consequent hydraulic properties were taken as basis for the simulations.

The lysimeter and the surrounding area of approximately 50 m x 50 m were permanently covered by grass. The grass was cut about twice a month during the vegetation period and irrigated about twice a week during summer, but shorter or longer non-irrigated and rainless periods can also be found (for three weeks in the growing season). Therefore there were basically well watered conditions in the growing season due to the irrigation, but periods with water scarcity (non-reference conditions) can also be found. In the dormant season there were even longer periods without irrigation. Maintenance also included manual clearing from weed and fertilization with long-term compound fertilizer for lawns.

Evapotranspiration ($ETO_{lys}$) was determined by considering soil water within the lysimeter ($W_{lys}$) and fluxes across its boundaries such as drainage ($W_{drain}$), evapotranspiration ($ETO_{lys}$), and precipitation ($P_{lys}$) and irrigation ($I_{lys}$).

To determine $W_{lys}$, nominal lysimeter weight was measured using a weighing facility. A mechanical system transformed the weight to an electronic load cell with an accuracy of ±0.2 kg (Nolz et al., 2013a). The analog output signal was amplified, converted to digital units, averaged and stored on a local server. Logging intervals were 15 and 10 minutes from 2004 to 2009 and from 2009 to 2011, respectively. The raw values (digital units) were converted into nominal mass (kg) using a calibration factor (Nolz et al., 2013a). It has to be noted that the calibrated weighing data represent relative lysimeter mass in kg, defined as current mass minus an unknown reference mass. Hence, only mass changes were determined. Dividing the nominal mass by the surface area ($m^2$) resulted in soil water equivalent ($W_{lys}$ / mm). Drainage water was measured at the bottom outlet of the lysimeter using a tipping bucket. Tipping and weighing data were logged at the same time intervals. Counts of tipping were converted into outflow data using a calibration factor (Nolz et al., 2013a). Dividing by the surface area resulted in drainage water ($W_{drain}$/mm). Soil water and drainage water were linked to a nominal time series ($W_{lys} + W_{drain}$), which was smoothed using a specific procedure (Nolz et al., 2013b; Nolz et al., 2014).

Equation (1) illustrates the relation between measured ($W_{lys} + W_{drain}$) and unknown ($P_{lys}$, $I_{lys}$, $ETO_{lys}$) water balance components.

$$\Delta(W_{lys} + W_{drain}) = (P_{lys} + I_{lys}) - ETO_{lys} \quad (1)$$

Therein $\Delta(W_{lys} + W_{drain})$ represents changes in soil water due to boundary fluxes (evapotranspiration $ETO_{lys}$, and precipitation $P_{lys}$ plus irrigation $I_{lys}$).

Accordingly, negative values of $\Delta(W_{lys} + W_{drain})$ – referring to a time interval of 10 or 15 minutes – were attributed to evapotranspiration under reference conditions (Nolz et al., 2014). Evaporation and interception losses were not considered. $ETO_{lys}$ was then processed to a daily time series ($ETO_{lys}$ / mm $d^{-1}$), with each day lasting from 7 a.m. to 7 a.m. of the following day. Finally, evapotranspiration as well as weather and data covering the years 2004 to 2011 were processed as monthly sums.

**Model description**

The Thornthwaite-type water balance model represents a 1-D system, considering only vertical fluxes. Input values are monthly precipitation (*PM*) (mm $month^{-1}$) and mean monthly temperature (*TM*) (°C) according to Thornthwaite (1955). Dingman (2002) slightly modified the original model, which has been applied as a basis. All input data (monthly sums from 2004 to 2011) originate from the experimental site in Groß-Enzersdorf; irrigation amounts of the lysimeter were added to precipitation.

The first step in setting up the model was the calculation of the potential evapotranspiration (*PET*). A temperature-based PET-model after Hamon (1964) was applied (Eq. 2):

$$PET_H = 29.8D\frac{e^*}{T_D + 273.2} \tag{2}$$

with

$$e^* = 0.611\exp\left(\frac{17.3T_D}{T_D + 237.3}\right) \tag{3}$$

where $D$ is the daylight hours (h $day^{-1}$), $T_D$ is the daily average temperature (°C), $e^*$ is saturation vapor pressure (kPa).

$PET_H$ from daily time-step was aggregated to monthly sum, noted $PET_{MH}$ (mm $month^{-1}$).

The following Equations (4–10) of this sub-chapter originated from Dingman (2002): When monthly precipitation ($P_M$) exceeds $PET_{MH}$, soil water storage is assumed to sufficiently provide vegetation with water and therefore *ET* is at its potential rate (Eq. 4):

$$\text{If } P_M \geq PET_{MH} \tag{4}$$

$$\text{then } ET_M = PET_{MH} \tag{5}$$

$$SOIL_M = \min\left\{\left[\left(P_M - ET_M\right) + SOIL_{M-1}\right],\ SOIL_{MAX}\right\} \tag{6}$$

where $ET_M$ (mm $month^{-1}$) is the monthly actual evapotranspiration, and $SOIL_M$ (mm $month^{-1}$) is the monthly soil moisture representing the amount of soil water that is available for the vegetation (not the total amount of soil water). $SOIL_{MAX}$ (mm $month^{-1}$) was introduced by considering unsaturated hydraulic parameters of the lysimeter soil type and rooting depth:

$$SOIL_{MAX} = \left(\theta_{fc} - \theta_{pwp}\right)z_{rz} \tag{7}$$

where: $\theta_{fc}$ is the water content at field capacity [$m^3/m^3$], $\theta_{pwp}$ is the water content at permanent wilting point [$m^3/m^3$] and $z_{rz}$ is the rooting depth (vertical extent of rooting zone in mm), the standard value is 1000 mm.

Both $ET_M$ and $SOIL_M$ denote the result parameters of the presented study.

For the simulation procedure, the first $SOIL_{M-1}$ value was set to a maximum value that corresponded with the soil-water storage capacity ($SOIL_{MAX}$). The basic assumption was that soil water storage is completely filled at the beginning of each vegetation period.

Values for $\theta_{fc}$ and $\theta_{pwp}$ were estimated based on the texture of the soil in the lysimeter using a pedotransfer function according to Baumer (1992). Input values are soil particle fractions (sand, silt, clay), bulk density (1.5 g $cm^{-3}$ in our case), and humus content (1% in this study).

The soil water was considered as storage reservoir used for evapotranspiration under condition of

$$P_M < PET_{MH} \tag{8}$$

$$\text{then: } ET_M = P_M + \Delta SOIL \tag{9}$$

$$\text{where: } \Delta SOIL = SOIL_{M-1} - SOIL_M = SOIL_{M-1}*\left(1 - \exp\left(-\frac{PET_{MH} - P_M}{SOIL_{MAX}}\right)\right) \tag{10}$$

with $\Delta SOIL$, the difference in the soil water storage (mm $month^{-1}$).

**Model calibration and validation**

Evapotranspiration data of the grass-covered lysimeter served as basis for calibration and validation. It is important to note that the model was not calibrated for drainage. However, drainage term can be calculated with the help of the model results.

In case of the lysimeter, runoff is not likely, thus only the recharge remains according to the following equation:

$$R = P_M - ET_M - \Delta SOIL \tag{11}$$

This equation is for the average monthly "water surplus" (i.e., the available water for recharge and runoff) (Dingman, 2002 pp. 316).

The available time series (2004–2011) was divided into two parts, whereof the first (2004–2008) was used for calibration and the second (2009–2011) for validation.

The first step of calibration considered potential evapotranspiration for actual land cover (i.e. periods when potential evapotranspiration values were close to actual evapotranspiration) using $ETO_{lys}$-values at well-watered (relative high soil moisture) conditions. The latter were assumed to occur when precipitation ($P_M$) exceeded potential evapotranspiration ($PET_{MH}$) or actual evapotranspiration ($ETO_{lys}$) exceeded potential evapotranspiration ($PET_{MH}$).

The $ETO_{lys}$-values selected in such a way are denoted $PETO_{lys}$. Measured $PETO_{lys}$ values (response variable) were correlated with calculated $PET_{MH}$ values (explanatory variable).

The regression line demonstrates the correlation between $PET_{MH}$ and $PETO_{lys}$ and with the slopes of a broken-line regression - as a calibration parameter - we can determine the calibrated Hamon type potential evapotranspiration ($PET_M$) (Figure 2). It is important to note that $PET_{MH}$ is the Hamon type, globally calibrated, calculated, while $PET_M$ is the locally calibrated potential evapotranspiration (for the study area). Due to the various state of the vegetation, *PET* of the dormant and the growing seasons are not the same, therefore different relationships had to be established for both parts (Rao et al., 2011). For this purpose, a software package named 'segmented' in the 'R' software environment was applied (R Core Team, 2012). The broken-line or segmented models create a piecewise linear relationship between the response and one or more of the ex-

planatory variables. This linear relationship is represented by two or more straight lines connected at unknown values called breakpoints (Muggeo, 2008). The basic principle was that when $PET_{MH}$ is equal to 0, then $PETO_{LYS}$ is 0 as well. The correlation between $PET_{MH}$ and $PETO_{LYS}$ cannot be described with a simple regression line, since the large lack of fit, and we did not want to use more complicated function. Consequently, broken-line regression was chosen.

The second step of the calibration is the estimation of the calibrated $SOIL_{MAX}$ parameter using $ETO_{LYS}$ data for the same (2004–2008) period. In this case, the initially estimated $SOIL_{MAX}$ parameter adjusted in order to reach minimum root mean square error between $ETO_{lys}$ and $ET_M$ by using the 'optim' function of 'R' software. (The range of this adjustment was from 10 mm to 1000 mm). Based on the value of $SOIL_{MAX}$ after the calibration, the vertical extent of the rooting zone (plant water uptake) was inversely estimated using soil texture data. The details of this estimation can be found in the Model Adjustment chapter.

Parameters of the calibration were considered for running the model with data of the validation period (2009–2011).

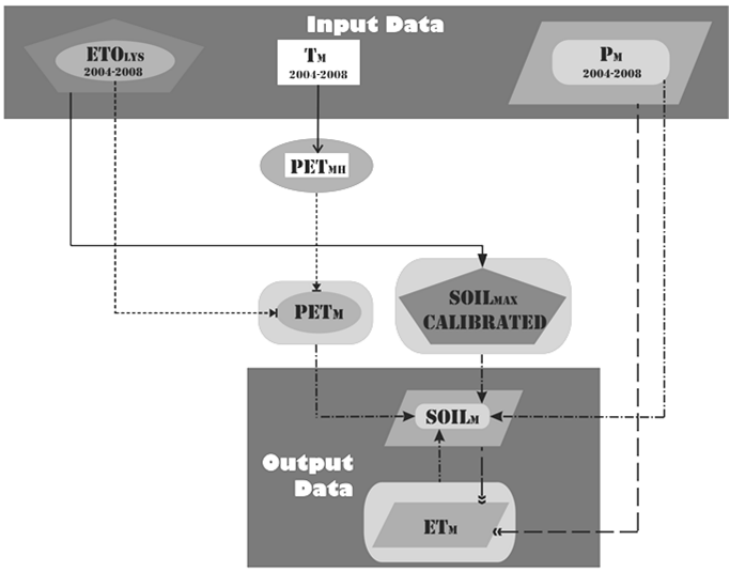


**Fig. 1.** Schematic representation of workflow of the modelling process including the relationships between input data, calculated and calibrated parameters, and output data. Parameters: $ETO_{LYS}$ is the measured actual evapotranspiration; $PET_{MH}$ is the Hamon type potential evapotranspiration; $PET_M$ is the calibrated potential evapotranspiration; $ET_M$ is the actual evapotranspiration, $SOIL_{MAX}$ *CALIBRATED* is the calibrated soil water storage-capacity of the soil, and $SOIL_M$ is the soil moisture. The different shapes with the different type of arrows illustrate the connections amongst the used parameters during the model workflow.

## Evaluating model performance

Model performance was evaluated using the Nash-Sutcliffe criterion, which is typical for calibrating and validating hydrologic models. In particular, it is suitable for models that simulate continuous time series of different time-period (Dingman, 2002). A proper model performance is presumed when the Nash-Sutcliffe coefficient, *NSE*, calculated according to Eq. 12, returns a value between 0.8 and 1.0:

$$NSE = 1 - \frac{\sum_{i=1}^{N}(ETO_{LYS\_i} - ET_{M\_i})^2}{\sum_{i=1}^{N}(ETO_{LYS\_i} - m_{ETO\_LYS})^2} \quad (12)$$

$ETO_{LYS\_i}$ is the time series of measured values, $ET_{M\_i}$ is the time series of simulated values and $m_{ET\_LYS}$: average value of $ETO_{LYS}$ for the period being measured.

## Projection procedure

*Regional climate models (RCMs)*

The validation of the model required the partition of the available dataset (2004–2011) into calibration (2004–2008) and validation periods (2009–2011). The original period of calibration however; was too short for the basis of the projection procedure, therefore we re-run the model using all available data. This re-run consequently means recalibration, therefore it delivered new and more reliable calibration parameters as well (Table 5). Here as much data as possible was assumed to deliver the best possible calibration relation. Nevertheless, there was small amount of data in the dormant season of the calibration (Figure 2).

Inputs for predicting future developments of $ET_M$ and $SOIL_M$ were the equation of the broken line regression, the calibrated $SOIL_{MAX}$ value, and predicted temperature and precipitation values. The latter originate from four grid-based, bias-corrected regional climate models (RCMs). Data were extracted from the nearest pixel to the experimental sites coordinates. The main properties of the RCMs can be found in Table 1. The underlying database called "FORESEE" contains daily meteorological data (min./max. temperature, and precipitation) based on ten RCMs for 2015–2100, and observation based data for the period 1951–2009, interpolated to 1/6×1/6 degree spatial resolution grid. The bias correction of the RCMs was done by a cumulative distribution functions fitting technique. This method corrected systematic errors in the RCM results. In case of precipitation, the intensity as well as the frequency of precipitation was corrected (Dobor et al., 2013).

In the following, each model is referred to as their model ID (first column of Table 1)

The RCMs time scale covers a range from 2015 to 2100. Each of them contains temperature and precipitation data in monthly time intervals. To evaluate the results for the 21st century, four main investigational periods were established: 1985–2015, 2015–2045, 2045–2075, and 2070–2100. With the data at hand, these 30-years-blocks with a 5-years overlap in the last two periods seemed the best partitioning. The overlap in the last part of the 21st century was necessary, because only 25 years of data were available.

**Table 1.** The applied RCMs (Linden van der and Mitchell, 2009).

| Model ID | Research Institute | Regional climate model | Driving general circulation model | Emission scenario | Spatial resolution |
|---|---|---|---|---|---|
| 1 | Max-Planck-Institute for Meteorology (MPI)* | REMO | ECHAM5 | A1B | 25km |
| 2 | Sweden's Meteorological and Hydrological Institute (SMHI)** | RCA | ECHAM5-r3 | A1B | 25km |
| 3 | Danish Meteorological Institute (DMI)*** | HIRHAM5 | ECHAM5 | A1B | 25km |
| 4 | Royal Netherlands Meteorological Institute (KNMI)**** | RACMO2 | ECHAM5-r3 | A1B | 25km |

*: Jacob (2001); **: Jones et al. (2004); ***: Christensen et al. (1996); ****: Lenderink et al. (2007)

**Table 2.** Annual mean values of temperature and precipitation derived from the regional climate models from 1985 to 2100 with standard deviations in parentheses In the first investigation period (1985–2015), the observation based averaged values (with standard deviations in parentheses) can be found.

| Model ID | Parameter | 1985/2015 | 2015/2045 | 2045/2075 | 2070/2100 |
|---|---|---|---|---|---|
| 1 | T [°C] | – | 11.0 (0.92) | 12.4 (0.89) | 13.3 (0.88) |
| | P [mm] | – | 653 (128) | 635 (99) | 692 (127) |
| 2 | T [°C] | – | 10.9 (0.84) | 12.1 (0.63) | 13.0 (0.73) |
| | P [mm] | – | 664 (106) | 743 (116) | 752 (122) |
| 3 | T [°C] | – | 11.1 (0.78) | 11.9 (0.87) | 12.6 (0.73) |
| | P [mm] | – | 587 (102) | 634 (122) | 653 (146) |
| 4 | T [°C] | – | 11.3 (0.69) | 12.3 (0.73) | 13.2 (0.84) |
| | P [mm] | – | 543 (127) | 585 (126) | 611 (115) |
| Average | T [°C] | 11.1 (0.76) | 11.1 (0.81) | 12.2 (0.78) | 13.0 (0.79) |
| | P [mm] | 606 (98) | 612 (116) | 649 (116) | 677 (127) |

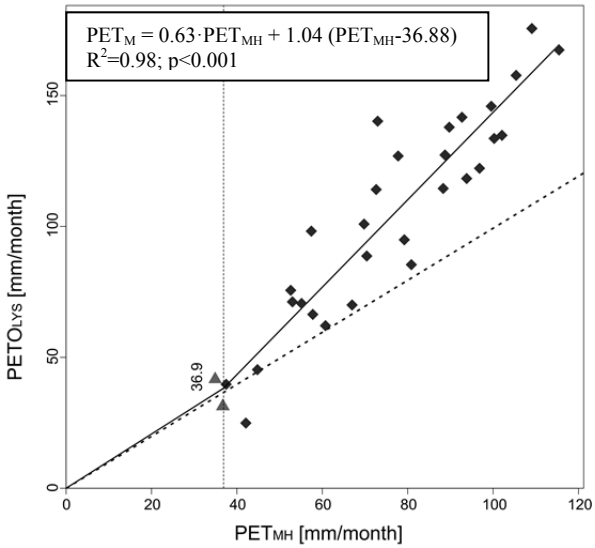


**Fig. 2.** Relationship between $PETO_{lys}$ and $PET_{MH}$ in dormant (to the left of the dotted vertical line) and growing season, with trend lines (solid) and 1:1 line (dashed).

The annual mean of temperature as well as precipitation showed an increasing tendency (+15% for T; +12% for P) at the end of the 21st century (Table 2). '1' had the highest, while '3' had the lowest value of temperature at the end of the investigation period. In the case of precipitation, '2' had the highest, but '4' had the lowest values. The values of '2' show the smallest deviation from the mean of the four RCMs in the context of temperature, while values of "3" demonstrate it in context of precipitation. However, '1' in general gives most representative values for Middle-Europe according to Dobor et al. (2013). Basic descriptive statistics were assessed for each of the periods and models.

*Rooting depth parameterisation for water stress conditions*

The sandy loam soil layer of the lysimeter ended at 1.4 m depth. For the second run, it was assumed that – under water stressed conditions – grass can use the water stored in the entire sandy loam soil profile. Consequently, for the second model run the parameter $z_{rz}$ (Eq. 7) was extended to a value representing the maximal possible rooting depth (1400 mm).

Potential stress conditions were determined for both basic and extended rooting depth.

In order to estimate periods with potential water stress, a simple water balance was established. The resulting values – calculated as potential *PET* minus $SOIL_M$ – are illustrated in Figure 8. Potential water stress is defined to occur if the deficits are positive and else exceeding soil moisture values.

## RESULTS AND DISCUSSION

### Model calibration and validation

Plotting monthly values of evapotranspiration from lysimeter measurements ($PETO_{lys}$) against values estimated using the Hamon approach ($PET_{MH}$) revealed that $PET_{MH}$ considerably underestimated the evapotranspiration measured with the lysimeter (Fig. 2). Correlation during the period of dormancy is illustrated by the section on the left of the vertical dotted line (broken-line approach); however, only two values of lysimeter data (triangles) could be related to this period, so little conclusion can be drawn from that. With regard to a better accordance, the correlation parameters of Figure 2 and Table 3 were utilised to obtain calibrated potential evapotranspiration values for the model ($PET_M$).

**Table 3.** Results of the broken-line regression.

| Segments | Estimated slope | Std. Error | *t* value | *Pr*(>\|*t*\|) |
|---|---|---|---|---|
| first | 0.63 | 0.31 | 1.88 | NA* |
| second | 1.04 | 0.34 | 3.35 | $2.3 \cdot 10^{-4}$ |

*Pr*(>|*t*|) is the p-value of the hypothesis testing of the slope. The null-hypothesis is that the slope is equal with 0. Because the p-value in our case very small we can reject the null-hypothesis.
*not available, because standard asymptotes were not applicable

The respective *NSE* value was 0.88, indicating a proper performance of the ET-model.

$ET_M$ calculated using the weather data of the validation period (2009–2011) reflected good accordance with the measured lysimeters data ($ETO_{LYS}$) (Figure 4). The corresponding *NSE* value of 0.85 was similar to that of the calibration period and thus also satisfactorily. In general, calibrating *ET* data is recommended when using the Hamon approach, even though this is rarely addressed in similar studies (e.g., Keables and Mehta, 2010).

### Model adjustment

A renewed $SOIL_{MAX}$ value resulting from the 7-years long adjusted and re-calibrated period was utilized to calculate the rooting depth using $\theta_{fc}$ and $\theta_{pwp}$ data from Table 4 for the first run (basic rooting depth).

$SOIL_{MAX}$ was 142.4 mm as pointed out after the calibration, and therefore $z_{rz}$ was 890 mm (using iteration) for the first run (basic rooting depth). The interpolation was carried out iteratively for determining the location of the rooting depth between *PAW* values of 126.2 mm and 161.0 mm (Table 4).

The $SOIL_{MAX}$-value for the second run (extended rooting depth) was 233.4 mm, since the *PAW* value of the 0–140 cm profile was considered as $SOIL_{MAX}$ (Table 4). Therefore, the impact of the extended rooting (by analyzing the plant water

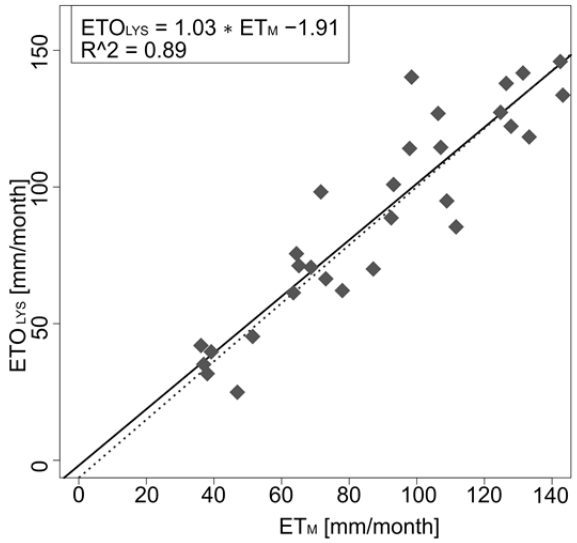


**Fig. 3.** Relationship between the calculated $ET_M$ and the measured $ETO_{lys}$ after calibration.

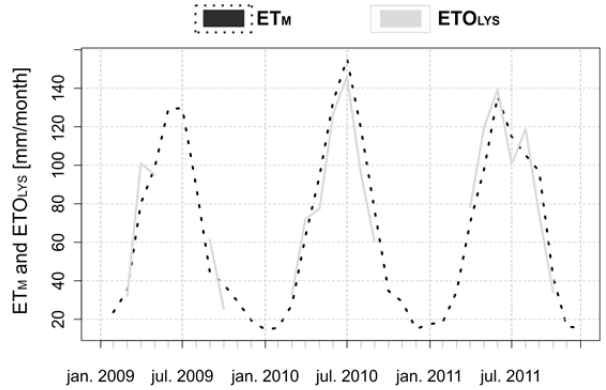


**Fig. 4.** Time series of the measured $ETO_{LYS}$ and calculated $ET_M$ values in the validation period.

uptake and water deficit stress) can be determined in order to evaluate potential adaption strategies of the plants to the warming.

**Projections**

Simulation results for both runs – run 1 with basic rooting depth and run 2 with extended rooting depth – are summarized in Table 6. Mean $ET_M$-values reproduce a slightly increasing trend, as would be expected from the predicted larger temperatures in the projection decades. However, it has to be noted that standard deviation was large. This indicates a large uncertainty that is inherent to modelled data, especially as four different RCMs were used in the given case. Differences depending on the input data are illustrated in Figure 5; the variation of $ET_M$ data between the four RCM models was substantial (10 mm in absolute values). '2' model reproduced the greatest increase as well as the largest values, because the respective RCM projects nearly 100 mm larger precipitation values for the 2045/75 period than the average. In contrast, the '4' model shows stagnancy in evapotranspiration and even a little decrease during the first run, since this model got the smallest values of precipitation. Comparing the first run (Figure 5a) with the second run (Figure 5b) reveals minor differences, which can be associated to the simulated availability of soil water. The latter, represented by averaged $SOIL_M$-values, followed an upward tendency (Table 6), mainly because of the underlying increasing precipitations.

With regard to plant water uptake, the minimal available soil water might be of interest. Therefore, minimum $SOIL_M$-values were calculated as 10$^{th}$ percentile minimums. The general trend of the respective $SOIL_{M\_MIN}$*10Percentile*-values was downwards (Figure 6) with remarkably larger values (16 mm in average) for the second run (Figure 6b). It is evident that the larger soil water storage capacity, as assumed for run 2, provided better conditions for plant growth. The four RCMs revealed a similar sequence as the $ET_M$-values in Figure 5. Only the '2' model deviates from the general pattern in the 2045/2075-period.

**Table 4.** The main properties of the soil profile in the lysimeter.

| Depth [cm] | $\theta_{fc}$ [vol-%] | $\theta_{pwp}$ [vol-%] | Plant available water (*PAW*) [vol-%] | Acc. *PAW** [mm] |
|---|---|---|---|---|
| 0–20 | 30.1 | 14.9 | 15.2 | 30.4 |
| 20–40 | 32.7 | 17.2 | 15.5 | 61.4 |
| 40–60 | 30.4 | 14.7 | 15.7 | 92.8 |
| 60–80 | 30.2 | 13.5 | 16.7 | 126.2 |
| 80–100 | 29.7 | 12.3 | 17.4 | 161.0 |
| 100–140 | 30.0 | 11.9 | 18.1 | 233.4 |
| 140–250 | 1.7 | 0.8 | 0.9 | -** |

*: Accumulated plant available water (*PAW*) accumulated to the bottom of the given layer [mm].
**: non-explainable

**Table 5.** The calibration parameters after the re-calibration.

| | |
|---|---|
| Result of the calibration of the PET | $PET_M = 0.54 \cdot PET_{MH} + 1.04$ ($PET_{MH}$–36.79) |
| Result of the calibration of the AET | $ETO_{LYS} = 1.04 \cdot ET_M - 2.36$ (*NSE* = 0.88) |

**Table 6.** $ET_M$, $SOIL_M$, and $SOIL_{M\_MIN}10^{th}$ *percentile* values with standard deviations for the two model runs.

| Parameters | 1985/2015 | 2015/2045 | 2045/2075 | 2070/2100 |
|---|---|---|---|---|
| | [mm] | [mm] | [mm] | [mm] |
| $ET_{M\ [basic\ rooting\ depth]}$ | 49 (34) | 49 (33) | 52 (34) | 53 (35) |
| $ET_{M\ [extended\ rooting\ depth]}$ | 50 (33) | 51 (32) | 53 (33) | 55 (33) |
| $SOIL_{M\ [basic\ rooting\ depth]}$ | 58 (40) | 65 (43) | 66 (44) | 67 (48) |
| $SOIL_{M\ [extended\ rooting\ depth]}$ | 92 (51) | 105 (57) | 105 (58) | 108 (64) |
| $SOIL_{M\_MIN}\ 10^{th}Percentile\ _{[basic\ rooting\ depth]}$ | 9 (3) | 7 (2) | 6 (3) | 5 (3) |
| $SOIL_{M\_MIN}\ 10^{th}Percentile\ _{[extended\ rooting\ depth]}$ | 26 (6) | 24 (7) | 22 (6) | 19 (7) |

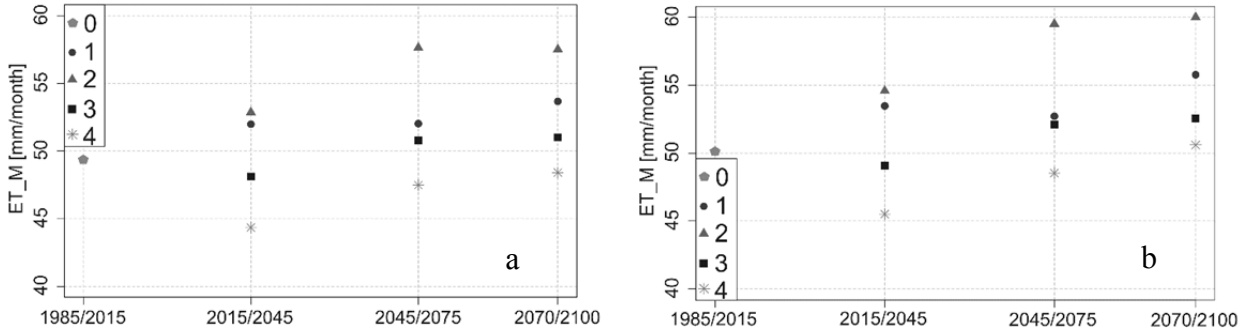


**Fig. 5.** The projected averages of evapotranspiration between 1985–2100; a: first run, and b: second run (the line represents the average).

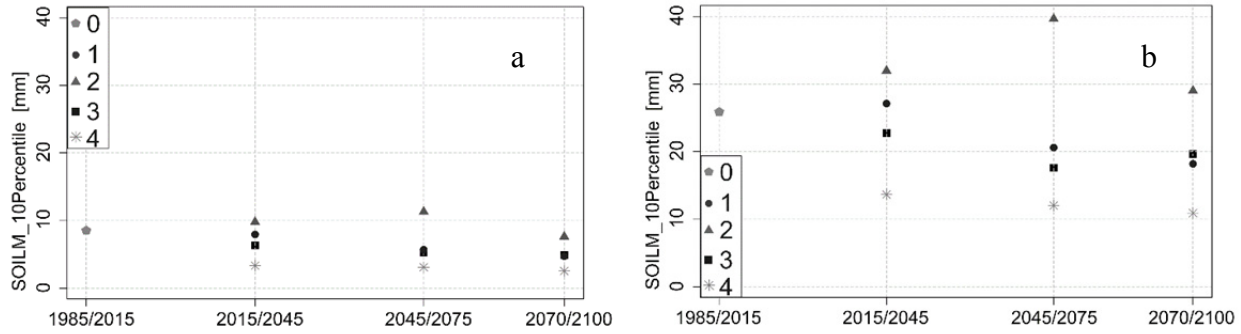


**Fig. 6.** The projected 10th percentile values of soil moisture between 1985–2100; a: first run, and b: second run. (The line represents average of the RCMs).

Model '1' represented the modelled averages of $ET_M$ and $SOIL_M$ at best in both runs.

In order to analyze seasonal trends, the annual course of $ET_M$ and $SOIL_M$ are illustrated in Figure 7 and Figure 8, respectively. The largest values of $ET_M$ appeared in June (95–100 mm for basic rooting depth; 98–105 mm for extended rooting depth). Smallest $SOIL_M$ can be found in September (12.5–25 mm for basic rooting depth; 50–60 mm for extended rooting depth), which is typical after summer and the end of the vegetative period. The largest values of $SOIL_M$ appeared in March – at the end of the dormancy and after winter precipitation. Consequently, also the decrease of soil moisture from April to August can be typically explained by plant water uptake (Figure 7 and 8).

Beside the evident seasonal trend, Figure 8 illustrates a shift of moisture between summer and winter. While $SOIL_M$-values predicted for the period 2070/2100 are largest in winter (in relation to the other projections), $SOIL_M$ appears smallest during summer. The reason may be found on the higher precipitation rate, which will assure the replenishment of soil moisture in the dormant season, while the increasing temperature will implicate greater evapotranspiration and consequently higher rate of water consumption by the plants on the growing season. For comparison, Calanca et al. (2006) project for the period 2070–2100 a reduction in summer soil moisture over most of Europe based on GCMs with a comparatively rough spatial resolution.

With respect to the basic rooting depth as considered for run 1, potential water stress was pronounced from June to September with the largest deficit in July, when $ET_M$ is at maximum and $SOIL_M$ is low (Figure 8a). Comparing the projection periods, the deficit is assumed to increase in future: For the 2070/2100 period it was approximately 50 mm in run 1, for instance. Consequently, periods of water stress are assumed to occur more often and shortage of the available water is assumed to increase, although more soil water might be available in total (Table 6). Similarly, Heinrich and Gobiet (2012) projected an increasing risk of dry spells for the period 2012–2050, as indicated by a negative Palmer Drought Severity Index. For the agricultural production in this area this could require adapted irrigation strategies in order to endure drought periods without loss of yield.

The larger $SOIL_{MAX}$-value of run 2 entailed larger $SOIL_M$-values (Figure 8b). As a consequence, deficit stress did not occur under these simulation preconditions. However, this hypothetical approach illustrates just the potential of reducing stress effects by improving or more efficiently using soil water storage capacity, since not only the rooting depth, but the seasonal development of aboveground biomass may change in future as well.

Nevertheless, the model works also on 1.4 m rooting depth, even if most roots are on the top 30 centimeters, and only a few located on deeper. According to Candell et al. (1996) crops can grow their roots even deeper, therefore the average of the maximum rooting depth for the globe is 2.1 ± 0.2 m in case of croplands and 2.6 ± 0.1 m for herbaceous plants.

Soil temperature is closely related to, and dependent on air temperature (Zheng et al., 1993). The projected increase in average surface temperature may also result in increased soil temperatures (IPCC, 2014), but it is more complex than the analogous changes in air temperature, since soil temperature is influenced by various factors (such as soil texture and moisture properties, the actual surface cover) (Jungvist et al., 2014). Root development may be affected directly by elevated soil temperatures, indirectly (e.g. changes in the physiology etc.) or by a mixture of those factors. Raised temperature triggers root growth rate up to a species-specific temperature optimum, and considerably alters several root architecture parameters (Gray and Bradya, 2016).

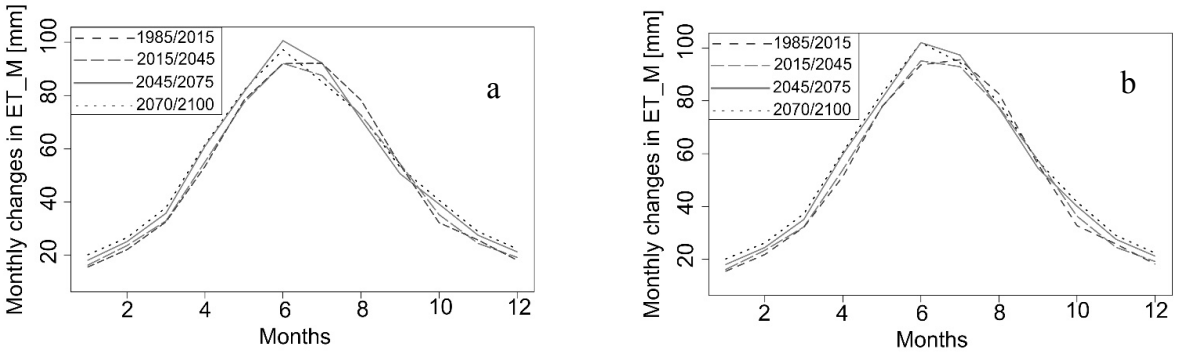


**Fig. 7.** Seasonal changes (mean annual courses of the different periods) of $ET_M$ in the projection periods; a: first run, and b: second run.

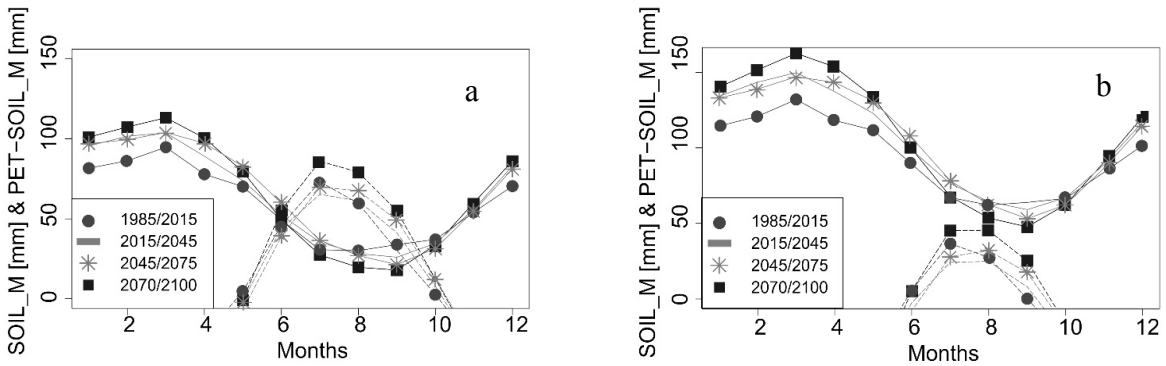


**Fig. 8.** Seasonal course (mean annual courses of the different periods) of $SOIL_M$ in the projection periods (solid lines) and estimated water deficit calculated as potential $ET$ minus $SOIL_M$ (dashed lines); a: first run, and b: second run.

After intensive reviews of the scientific literature, specifically similar studies have not been found, which are exactly comparable to this work. The mentioned studies in the Introduction, namely Eitzinger et al., 2003, 2013; Strauss et al., 2012 and Thaler et al., 2012 have done crop simulations in context of water stress at Marchfeld, while in this article the grass covered surfaces was in the focus.

Nevertheless, there are impact analysis studies of water balance models (e.g., Keables and Mehta, 2010; Lutz et al., 2010; Mohammed et al., 2012; Remrová and Císlerová, 2010; Zamfir 2014) as referred in earlier, which also demonstrated that the evapotranspiration may increase, but the soil water content may decrease in the future due to the apparently increasing temperature and the decreasing precipitation. They applied mainly Thornthwaite-type, monthly-step water balance model, but basically evaluate their results annually, instead of monthly or seasonal scale as in this study. In case of their study areas there are various climates, different climate models (i.e. GCMs or RCMs), and emission scenarios with not the same investigation time series. Climate change impact studies are nevertheless always affected by uncertainties, particularly in climate model scenarios with regard to climate variability (Eitzinger et al., 2003) which makes also the comparison more difficult.

## CONCLUSIONS

In this study, a Thornthwaite-type water balance model was adapted and applied to assess the future development of evapotranspiration and soil moisture in an agricultural area in the eastern part of Austria. The key new model aspect was on one hand the two-stage evapotranspiration calibration process (calibration of potential, and the calibration of the actual evapotranspiration separately). On second hand the adaption of the broken-line regression method in the calibration of the potential evapotranspiration.

The main finding was that both $ET$ and $SOIL_M$ were predicted to become larger in future decades when assuming the results of standard climate scenarios. The remarkable shift predicted for $SOIL_M$ indicates that less soil water will be available during summer months in future. This outcome was underlined when estimating stress conditions based on periods with a negative water balance. The results of a second scenario with an extended rooting depth (i.e., larger $SOIL_{MAX}$ value) indicated that such stress periods could be avoided if the plants were able to utilize available soil water below a depth of 1 m.

The results also indicate that increasing soil water storage capacity can be an adequate adaption strategy to mitigate climate change effects in the investigated area. However, the presented simulations only provide some baseline investigations, where a relatively straightforward model approach was adapted to regional conditions and applied. Nevertheless, the developed model involves low amount of input data (precipitation and temperature); therefore it could easily be extended to larger regional scale, which requires a significant lower amount of work for input data' preprocessing for some baseline investigations than more complex models. The use of only two input parameters enables a much easier uncertainty analysis of the applied model as well. Furthermore, it ensures fast impact analysis of climate change on evapotranspiration and soil water storage.

*Acknowledgement*. The project was supported by EFOP-3.6.2-16-2017-00018 for the University of Sopron project.

## REFERENCES

Baumer, O.W., 1992. Predicting unsaturated hydraulic parameters. In: van Genuchten, M.Th., Leij, F.J. (Eds.): Proceedings of the international workshop on Indirect methods for estimating the hydraulic properties of unsaturated soils. Riverside, California, October 11–13, 1989, 341–354.

Calanca, P.L., Roesch, A., Jasper, K., Wild, M., 2006. Global warming and the summertime evapotranspiration regime of the Alpine region. Climatic Change, 79, 65–78.

Canadell, J., Jackson, R.B., Ehleringer, J.B., Mooney, H.A., Sala, O.E., Schulze, E.-D., 1996. Oecologia, 108, 4, 583–595. https://doi.org/10.1007/BF00329030

Christensen, J.H., Christensen, O.B., Lopez, P., Van Meijgaard, E., Botzet, M., 1996. The HIRHAM4 regional atmospheric climate model, DMI Technical Report 96-4. Available from DMI, Lyngbyvej 100, Copenhagen Ø.

Dingman, L.S., 2002. Physical Hydrology. Prentice-Hall, New Jersey, USA, 646 p.

Dobor, L., Barcza, Z., Hlásny, T., Havasi, Á., 2013. Creation of the FORESEE database to support climate change related impact studies. International Scientific Conference for PhD Students.

Eitzinger, J., Štastná, M., Žalud, Z., Dubrovsky, M., 2003. A simulation study of the effect of soil water balance and water stress on winter wheat production under different climate change scenarios. Agricultural Water Management, 61, 195–217.

Eitzinger, J., Thaler, S., Schmid, E., Strauss, F., Ferrise, R., Moriondo, M., Bindi, M., Palosuo, T., Rötter, R., Kersebaum, K.C., Olesen, J.E., Patil, R.H., Şaylan, L., Çaldağ Çaylak, O., 2013. Sensitivities of crop models to extreme weather conditions during flowering period demonstrated for maize and winter wheat in Austria. The Journal of Agricultural Science, 151, 6, 813–835. DOI: 10.1017/S0021859612000779.

Götz, B., Hadatsch, S., Kratochvil, R., Vabitsch, A., Freyer, B., 2000. Biologische Landwirtschaft im Marchfeld. Potenziale zur Entlastung des Natur- und Landschaftshaushaltes. Umweltbundesamt GmbH, Vienna.

Gray, S.B., Bradya, S.M., 2016. Plant developmental responses to climate change. Developmental Biology, 419, 64–77. https://doi.org/10.1016/j.ydbio.2016.07.023

Hamon, W.R., 1964. Computation of direct runoff amounts from storm rainfall. Intl. Assoc. Scientific Hydrol. Publ., 63, 52–62.

Herceg, A., Kalicz, P., Kisfaludi, B., Gribovszki, Z., 2016. A monthly-step water balance model to evaluate the hydrological effects of climate change on a regional scale for irrigation design. Slovak Journal of Civil Engineering, 24, 4, 27–35. DOI: 10.1515/sjce-2016-0019.

Heinrich, G., Gobiet, A., 2012. The future of dry and wet spells in Europe: A comprehensive study based on the ENSEMBLES regional climate models. Int. J. Climatol., 32, 1951–1970.

IPCC, 2007. Climate change 2007. Impacts, adaptation and vulnerability. In: Parry, M.L., Canziani, O.F., Palutikof, J.P., van der Linden, P.J., Hanson, C.E., (Eds.): Contribution of Working Group II to the Fourth Assessment Report of the Intergovernmental Panel on Climate Change. Cambridge University Press, Cambridge, UK and New York, NY, USA, 976 p.

IPCC, 2014. Climate Change 2014. Synthesis Report. Contribution of Working Groups I, II and III to the Fifth Assessment Report of the Intergovernmental Panel on Climate Change [Core Writing Team, Pachauri R.K., Meyer L.A. (Eds.)]. IPCC, Geneva, Switzerland, 151 p.

Jacob, D., 2001. A note to the simulation of the annual and inter-annual variability of the water budget over the Baltic Sea drainage basin. Meteorol. Atmos. Phys., 77, 61–73.

Jones, C.G., Ullerstig, A., Willen, U., Hansson, U., 2004. The Rossby Centre regional atmospheric climate model (RCA). Part I: model climatology and performance characteristics for present climate over Europe. Ambio, 33, 4–5, 199–210.

Jungvist, G., Oni, S.K., Teutschbein, C., Futter, M.N., 2014. Effect of climate change on soil temperature in Swedish boreal forests. PLoS One, 9, 4, e93957. https://doi.org/10.1371/journal.pone.0093957

Keables, M.J., Mehta, S., 2010. A soil water climatology for Kansas. Great Plains Research, 20, 2, 229–248.

Lenderink, G., Buishand, A., Van Deursen, W., 2007. Estimates of future discharges of the river Rhine using two scenario methodologies: direct versus delta approach. Hydrol. Earth Syst. Sci., 11, 1145–1159. DOI: 10.5194/hess-11-1145-2007.

van der Linden, P., Mitchell, J.F.B. (Eds.), 2009. ENSEMBLES: Climate Change and its Impacts: Summary of research and results from the ENSEMBLES project. Met Office Hadley Centre, FitzRoy Road, Exeter EX1 3PB, UK.

Lutz, J.A., Wagtendonk, J.W., Franklin, J.F., 2010. Climatic water deficit, tree species ranges, and climate change in Yosemite National Park. Journal of Biogeography, 37, 936–950.

Mohammed, R.K., Mamoru, I., Motoyoshi, I., 2012. Modeling of seasonal water balance for crop production in Bangladesh with implications for future projection. Ital. J. Agron., 7, 2, 146–153.

Muggeo, V.M.R., 2008. Segmented: An R package to fit regression models with broken-line relationships. R News, The Newsletter of the R Project, 8, 1, 20–25.

Nachtnebel, H.P, Dokulil, M., Kuhn, M., Loiskandl, W., Sailer, R., Schöner, W., 2014. Influence of climate change on the hydrosphere. In: Austrian Panel on Climate Change (APCC) Austrian Assessment Report Climate Change 2014 (AAR14). Austrian Academy of Sciences Press, Vienna, pp. 411–466.

Neuwirth, F., Mottl, W., 1983. Errichtung einer Lysimeteranlage an der agrar-meteorologischen Station in Groß-Enzersdorf. Wetter und Leben, 35, 48–53.

Nolz, R., Kammerer, G., Cepuder, P., 2013a. Interpretation of lysimeter weighing data affected by wind. J. Plant Nutr. Soil Sci., 176, 200–208.

Nolz, R., Kammerer, G., Cepuder, P., 2013b. Improving interpretation of lysimeter weighing data. Die Bodenkultur: Journal for Land Management, Food and Environment 64, 27–35.

Nolz, R., Cepuder, P., Kammerer, G., 2014. Determining soil water-balance components using an irrigated grass lysimeter in NE Austria. J. Plant Nutr. Soil Sci., 177, 237–244.

Nolz, R., Cepuder, P., Eitzinger, J., 2016. Comparison of lysimeter based and calculated ASCE reference evapotranspiration in a sub-humid climate. Theor. Appl. Climatol., 124, 1, 315–324.

Rao, L.Y., Sun, G., Ford, C.R., Vose, J.M., 2011. Modeling potential evapotranspiration of two forested watershed in the southern appalachians. Trans. ASABE, 54, 6, 2067–2078.

R Core Team, 2012. R: A language and environment for statistical computing. R Foundation for Statistical Computing, Vienna, Austria. http://www.R-project.org/.

Remrová, M., Číslerová, M., 2010. Analysis of climate change effects on evapotranspiration in the watershed Uhlířská in the Jizera mountains. Soil & Water Research, 5, 1, 28–38.

Strauss, F., Schmid, E., Moltchanova, E., Formayer, H., Wang, X., 2012. Modeling climate change and biophysical impacts of crop production in the Austrian Marchfeld Region. Climate Change, 111, 641. https://doi.org/10.1007/s10584-011-0171-0

Sun, G.K., Alstad, J., Chen, S., Chen, C.R., Ford, G., Lin, C., Liu, N., Lu, S.G., McNulty, H., Miao, A., Noormets, J.M., Vose, B., Wilske, M., Zeppel, Y., Zhang, Z., 2010. A general projective model for estimating monthly ecosystem evapotranspiration. Ecohydrol., 4, 2, 245–255.

Thaler, S., Eitzinger, J., Trnka, M., Dubrovsky, M., 2012. Impacts of climate change and alternative adaptation options on winter wheat yield and water productivity in a dry climate in Central Europe. The Journal of Agricultural Science, 150, 5, 537–555. DOI: 10.1017/S0021859612000093.

Thornthwaite, C.W., Mather, J.R., 1955. The Water Balance. Drexel Institute of Technology, Climatological Laboratory Publication 8. Philadelphia, USA.

Zamfir, R.H.C., 2014. The impact of climate changes on water balance from western Romania using computer tools. In: Niola, V. (Ed.): Recent Advances in Energy, Environment, Biology and Ecology. World Scientific and Engineering Academy and Society. ISBN: 978-960-474-358-2.

Zheng, D., Hunt, E.R., Running, S.W., 1993. A daily soil temperature model based on air temperature and precipitation for continental applications. Clim. Res., 2, 183–191. DOI: 10.3354/cr002183.

Received 17 May 2018
Accepted 18 March 2019